Journal of Materials Chemistry A

RSC Publishing

PAPER

View Article Online
View Journal | View Issue

Nitrogen-doped layered oxide $Sr_5Ta_4O_{15-x}N_x$ for water reduction and oxidation under visible light irradiation†

Cite this: *J. Mater. Chem. A*, 2013, **1**, 5651

Shanshan Chen,[ab] Jingxiu Yang,[ab] Chunmei Ding,[ab] Rengui Li,[ab] Shaoqing Jin,[ab] Donge Wang,[a] Hongxian Han,[a] Fuxiang Zhang*[a] and Can Li*[a]

Development of a photocatalyst with wide visible light absorption is of vital importance in solar-chemical energy conversion. In this work, we introduce a new nitrogen-doped layered oxide, $Sr_5Ta_4O_{15-x}N_x$, which exhibits a significantly extended absorption edge compared with the undoped oxide $Sr_5Ta_4O_{15}$. The extension of the visible light absorption has been ascribed to the substitution of nitrogen for oxygen atoms as well as the formation of Ta–N bonds, which was confirmed by X-ray diffraction (XRD) patterns, X-ray photoelectron spectroscopy (XPS) and Raman spectroscopy. Judged by the first principle calculation, the N 2p states mixed with pre-existing O 2p states shift the valence band maximum upward and result in wide visible light absorption. Band structure analysis combined with UV-Vis diffuse reflectance spectrum (DRS) and Mott–Schottky (M–S) measurement shows that the conduction and valence bands of $Sr_5Ta_4O_{15-x}N_x$ are sufficient for water reduction and oxidation, respectively. The photocatalytic water splitting performances of $Sr_5Ta_4O_{15-x}N_x$ are strongly related to the deposited cocatalyst. With an optimized cocatalyst, the $Sr_5Ta_4O_{15-x}N_x$ shows both H_2 and O_2 evolution activities under visible light irradiation using CH_3OH and $AgNO_3$ as scavengers respectively. Following the optimized cocatalyst deposition of the $Sr_5Ta_4O_{15-x}N_x$, the cocatalyst-modified nitrogen-doped tantalum-based layered oxides $Sr_2Ta_2O_{7-x}N_x$ and $Ba_5Ta_4O_{15-x}N_x$ also exhibit activities for both the water splitting half reactions. This work demonstrates that the nitrogen-doped tantalum-based layered oxides may be a new type of potential photocatalyst with wide visible light absorption for solar water splitting.

Received 30th January 2013
Accepted 28th February 2013

DOI: 10.1039/c3ta10446j

www.rsc.org/MaterialsA

1 Introduction

Photocatalytic splitting of water into hydrogen and oxygen using a heterogeneous photocatalyst is a potentially clean and renewable solution to convert solar energy into hydrogen fuel.[1] In this field, one of the most important issues is the development of suitable semiconductors as photocatalysts. During the past decades, a large number of semiconductors have been reported to be active for water splitting.[1c,2] However, most of them only function under UV irradiation owing to their wide band gaps. From the viewpoint of both fundamental understanding and practical applications, it is extremely important to develop potential photocatalysts which simultaneously satisfy the following requirements: (i) harvest a wide range of visible photons to utilize the main part of the solar spectrum; (ii) possess sufficient negative (positive) potential of the conduction (valence) band to obviously drive water reduction (oxidation) in the presence of suitable electron donors (acceptors); (iii) remain stable in water under irradiation.

In order to overcome the limitation of the majority of oxides that they are only UV responsive for water splitting, many methods have been developed to extend their light absorption into the visible region, such as metal ion(s) doping,[3] converting the oxides into (oxy)nitrides[4] and (oxy)sulfides,[5] and reduction of oxides.[6] For example, the visible-light-responsive materials TaON[4a,7] and $(Ga_{1-x}Zn_x)(N_{1-x}O_x)$[4d,8] have been extensively investigated for solar water splitting. Anion doping, especially nitrogen doping, is another efficient strategy to shift the optical response of oxides into the visible spectral range.[9] Several routes, including thermal treatment in an ammonia atmosphere, have been developed to realize the nitrogen doping.[10] However, the traditional micrometer-sized nitrogen-doped photocatalysts usually show weak absorption in the visible region due to the low content of nitrogen incorporated.[11] In order to increase the amount of the nitrogen doping and extend the visible light absorption, some methodologies have been applied, such as decreasing the particle size[12] and introduction of a second dopant.[13]

[a]State Key Laboratory of Catalysis, Dalian Institute of Chemical Physics, Chinese Academy of Sciences, Dalian National Laboratory for Clean Energy, Dalian 116023, P. R. China. E-mail: fxzhang@dicp.ac.cn; canli@dicp.ac.cn; Fax: +86-411-84694447; Tel: +86-411-84379070

[b]Graduate University of Chinese Academy of Sciences, Beijing 100049, P. R. China

† Electronic supplementary information (ESI) available: SEM and TEM images (S1, S5 and S6), H_2 evolution performance (S2), UV-Vis absorption spectra (S3), and XPS spectra (S4) for the $Sr_5Ta_4O_{15-x}N_x$ based photocatalysts. XRD patterns (S7 and S8) and time courses of H_2 (S9) and O_2 (S10) evolution for the $Ba_5Ta_4O_{15-x}N_x$ and $Sr_2Ta_2O_{7-x}N_x$ based photocatalysts. See DOI: 10.1039/c3ta10446j

Recently, the strategy of nitrogen doping has been efficiently extended to the oxides with a layered perovskite or tunnelled pyrochlore structure and their absorption range can be obviously broadened due to the easy diffusion of the dopant from the surface to the bulk through the interlayer or tunnel galleries, resulting in increased nitrogen incorporation.[14] A series of nitrogen-doped oxides, such as $Cs_{0.68}Ti_{1.83}O_{4-x}N_x$,[14a] $CsTaWO_{6-x}N_x$,[14c] $Sr_2Ta_2O_{7-x}N_x$,[15] $Ba_5Ta_4O_{15-x}N_x$[16] and $CsCa_2Ta_3O_{10-x}N_x$,[17] have been reported to possess wide visible light absorption, some of which even show an absorption edge exceeding 600 nm. To date, many of these nitrogen-doped oxides have been reported to be active either for H_2 or O_2 evolution from water in the presence of scavenger under visible light irradiation ($\lambda > 400$ nm). However, the photocatalyst that exhibits both half reaction activities has been limited to the recently reported layered $CsCa_2Ta_3O_{10-x}N_x$.[17,18] It is desirable to explore more nitrogen-doped layered oxides that can obviously drive both water reduction and oxidation half reactions under visible light irradiation.

Tantalum-based photocatalysts have attracted great interest in the field of solar water splitting. So far more than thirty tantalum-based oxides have been reported to be active for overall water splitting under UV irradiation, among which the $NaTaO_3$:La photocatalyst achieved an extremely high quantum efficiency of 56% at 270 nm.[19] In order to develop a visible-light-responsive photocatalyst for overall water splitting, some tantalum-based (oxy)nitrides, such as Ta_3N_5, TaON and $BaTaO_2N$, have been extensively investigated as potential photocatalysts because of their wide range of visible light absorption and stable performances to drive both water reduction and oxidation half reactions.[4a,b,e,20] In consideration of the success of the tantalum-based oxides for overall water splitting under UV light irradiation, it is expedient to develop more potential tantalum-based photocatalysts that can harvest visible light and drive two half reactions of water splitting.

Herein, we prepared a nitrogen-doped tantalum-based layered oxide $Sr_5Ta_4O_{15-x}N_x$ by nitriding the corresponding oxide precursor $Sr_5Ta_4O_{15}$ under an ammonia flow. After loading an optimized cocatalyst of Pt or CoO_x and under visible light irradiation, the $Sr_5Ta_4O_{15-x}N_x$ based photocatalyst is active for both photocatalytic water reduction and oxidation in the presence of CH_3OH and $AgNO_3$ respectively. The photocatalytic performances of water splitting are strongly related to the cocatalysts as well as their deposition methods, demonstrating their structure sensitivity to water splitting. Furthermore, we extended the strategy of the cocatalyst deposition to other nitrogen-doped tantalum-based layered oxides, $Sr_2Ta_2O_{7-x}N_x$ and $Ba_5Ta_4O_{15-x}N_x$, on which remarkable H_2 and O_2 evolution were also achieved under visible light irradiation. It demonstrates that the nitrogen-doped tantalum-based layered oxides may be promising visible-light-responsive photocatalysts for solar water splitting.

2 Experimental and calculation methods

2.1 Preparation of $Sr_5Ta_4O_{15-x}N_x$

$Sr_5Ta_4O_{15}$ was prepared by the polymerizable complex (PC) method reported in the literature.[21] The detailed experimental procedures are described in the ESI.† $Sr_5Ta_4O_{15-x}N_x$ was prepared by a thermal ammonalysis process. Typically, 0.7 g of as-synthesized $Sr_5Ta_4O_{15}$ was placed on a quartz basket padded with quartz wool and heated at 1123 K for 15 h under the ammonia flow (250 mL min^{-1}). After naturally cooling to room temperature, the sample was collected and stored in a desiccator for use.

2.2 Preparation of $Ba_5Ta_4O_{15-x}N_x$ and $Sr_2Ta_2O_{7-x}N_x$

The oxide precursors of $Ba_5Ta_4O_{15}$ and $Sr_2Ta_2O_7$ were both prepared by a conventional solid state reaction method according to the procedures reported in the literature.[15,16] Similarly, the $Ba_5Ta_4O_{15-x}N_x$ and $Sr_2Ta_2O_{7-x}N_x$ oxides were prepared by nitriding those oxide precursors. The corresponding nitridation temperature and time were at 1173 K for 150 min and 1183 K for 90 min, respectively.

2.3 Deposition of cocatalysts

2.3.1 Deposition of cocatalysts for H_2 evolution. The cocatalysts for H_2 evolution were deposited by conventional impregnation and subsequent H_2 reduction (denoted as Imp.-H_2). Typically, 0.2 g $Sr_5Ta_4O_{15-x}N_x$ was immersed in a *ca.* 2 mL aqueous solution containing metal precursor ($[(NH_4)_2Pt]Cl_6$, K_2IrCl_6 or $Na_3RhCl_6 \cdot 12H_2O$), and sonicated for *ca.* 10 min. After the solution was completely evaporated in a water bath at 353 K, the resulting powder was collected and reduced at 623 K for 2 h under a flow of 5% H_2/Ar (200 mL min^{-1}).

For comparison, *in situ* photodeposition (denoted as P.D.) was also adopted. Typically, a calculated amount of metal precursor ($[(NH_4)_2Pt]Cl_6$, K_2IrCl_6 or $Na_3RhCl_6 \cdot 12H_2O$) was added to the 150 mL aqueous reaction solution containing 0.15 g $Sr_5Ta_4O_{15-x}N_x$, 0.15 g La_2O_3 and 20 v% CH_3OH before irradiation. A 300 W Xenon lamp equipped with an optical filter (Hoya, L-42; $\lambda \geq 420$ nm) to cut off the ultraviolet light was used to irradiate the vacuum solution for 5 h. The Pt, Ir or Rh cocatalyst is expected to be formed in the early stage of irradiation by reacting with the photogenerated electrons.

2.3.2 Deposition of cocatalysts for O_2 evolution. Three kinds of cocatalysts were deposited for evaluation of water oxidation performance, which were denoted as CoO_x, CoO_x-(Imp.) and IrO_2 in this work. The CoO_x deposition procedure was referenced to the literature,[22] where the cobalt nitrate was impregnated onto the photocatalyst, and then calcined at 973 K for 1 h under ammonia flow. As for the deposition of CoO_x(Imp.), a calculated amount of cobalt nitrate solution was impregnated and calcined at 473 K for 2 h in the air instead of NH_3 flow. The preparation procedure of the IrO_2 colloid solution was referenced to previous literature.[22,23] As for the adsorption of IrO_2 colloid, a desired amount of $Sr_5Ta_4O_{15-x}N_x$ powder was added to this colloid solution with stirring for 1 h, and the mixture was then filtered and washed three times with distilled water. The filtered powder was dried at 333 K for use. The detailed description on the deposition of CoO_x and preparation of IrO_2 colloid solution is given in the ESI.†

2.4 Characterizations of catalysts

XRD measurement was carried out on a Rigaku D/Max-2500/PC powder diffractometer (Cu Kα radiation) with an operating voltage of 40 kV and an operating current of 200 mA. The scan rate of 5° min^{-1} or 1° min^{-1} was applied in the range of 5–60° or 27–34° at a step size of 0.02°. UV-Vis diffuse reflectance spectra (DRS) were recorded on a UV-Vis spectrophotometer (JASCO V-550) equipped with an integrating sphere, and $BaSO_4$ powder was used as the reference for baseline correction. The morphologies and particle sizes were examined by scanning electron microscopy (SEM; Quanta 200 FEG, FEI and S-5500, Hitachi) and transmission electron microscopy (TEM; HT7700, Hitachi). The Brunauer–Emmett–Teller (BET) surface area was measured at 77 K using a Micromeritics ASAP 2000 adsorption analyzer. The binding energies were determined by X-ray photoelectron spectroscopy (XPS, Thermo Esclab 250Xi, a monochromatic Al Kα X-ray source), and normalized to the C 1s peak (284.6 eV) for each sample, which 1 wt% Pt was deposited for the measurement in order to achieve clear signals. The content of the nitrogen dopant was analyzed using a flash elemental analyzer (HORIBA, EMGA-930). Pt contents were determined by inductively coupled plasma (ICP) mass spectrometry analysis. UV Raman spectra were measured at room temperature on a self-assembled UV Raman spectrograph with the spectral resolution of 2 cm^{-1}. 325 nm of the He–Cd laser with an output of 25 mW was used as the exciting source. The power of the laser at sample was *ca.* 3.0 mW.

2.5 Computational details

The DFT calculation has been performed by the VASP code.[24] The interaction between ions and electrons is described by the projector-augmented wave (PAW) method.[25] The PBE parameterization with GGA was adopted for the exchange correlation. The bulk lattice of $Sr_5Ta_4O_{15}$ was optimized by using 400 eV as cutoff energy and 5 × 5 × 3 Monkhorst–Pack *k*-point sampling.[21] The doping ratio (0.067) of N/O is referenced to the experimental result (0.042) and different nitrogen doping sites have been considered, which showed that substitution of O with N at O1 (0.5, 0, 0) was more energetically stable than at O2 (0.83, 017, 0.81) or O3 (0.34, 0.17, 0.39).

2.6 Photocatalytic reactions

The photocatalytic reactions were carried out in a Pyrex top-irradiation-type reaction vessel connected to a closed gas circulation system. A 150 mL aqueous solution containing 0.15 g photocatalyst was adopted, and 0.01 M $AgNO_3$ and 20 v% methanol were used as scavengers for photocatalytic water oxidation and reduction, respectively. 0.15 g La_2O_3 was added to maintain the pH value of the reaction solution, which was measured at *ca.* 8.5. Prior to photoirradiation, the reaction mixture was evacuated to ensure complete air removal, and then irradiated from the top side with a 300 W Xenon lamp using a filtration mirror which was equipped with an optical filter (Hoya, L-42; $\lambda \geq 420$ nm) to cut off the light in the ultraviolet region. A flow of cooling water was used to maintain the reaction mixture at room temperature. The evolved gases were analyzed by gas chromatography (Agilent; GC-7890A, MS-5A column, TCD, Ar carrier).

2.7 Electrochemical analysis

For the Mott–Schottky (M–S) measurement, $Sr_5Ta_4O_{15-x}N_x$ particles were deposited on FTO conducting glass by the electrophoretic deposition method. The area of the electrode was fixed to 0.36 cm^2 by insulating cement. The measurement was carried out on a CHI660B electrochemical workstation (Shanghai Chenhua Limited, China) using 0.1 M Na_2SO_4 (pH = 8.5, adjusted by NaOH) solution as the electrolyte.

3 Results and discussion

3.1 Structural characterizations of the $Sr_5Ta_4O_{15-x}N_x$

$Sr_5Ta_4O_{15}$ is a typical layered compound with TaO_6 octahedra connected by corner-sharing, and the tantalum oxide sheets are separated by strontium ions as interlayer counterions.[21] As shown in Fig. 1A, it contains two kinds of interlayers, one consists of four strontium ions and the other is composed of two strontium ions. After thermal ammonia treatment, the layered structure is maintained for $Sr_5Ta_4O_{15-x}N_x$ according to the X-ray diffraction (XRD) patterns shown in Fig. 1B. In addition, there is nearly no change in the crystal structure compared with the pristine $Sr_5Ta_4O_{15}$, except that the diffraction peak intensity of the $Sr_5Ta_4O_{15-x}N_x$ is slightly decreased. In order to further check the influence of ammonia treatment on the structure of the $Sr_5Ta_4O_{15}$, a much slower scanning rate was adopted to collect the main diffraction peaks located at 29.6° and 31.6°. As given in the inset of Fig. 1B, these diffraction peaks are both slightly shifted to smaller angles after the ammonia treatment, demonstrating that nitrogen atoms may

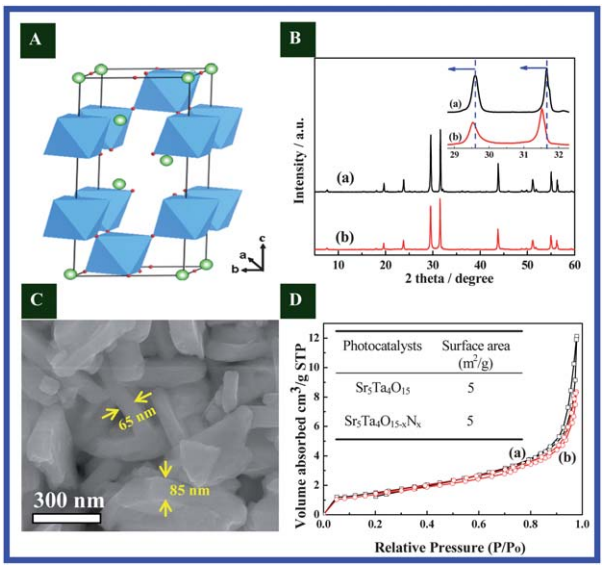

Fig. 1 Structural characterizations of $Sr_5Ta_4O_{15}$ (a) and $Sr_5Ta_4O_{15-x}N_x$ (b): (A) crystal structure model of $Sr_5Ta_4O_{15}$; (B) XRD patterns; (C) SEM image of $Sr_5Ta_4O_{15-x}N_x$; (D) adsorption–desorption isotherms.

have substituted the oxygen sites and incorporated into the $Sr_5Ta_4O_{15}$ lattice. The high possibility of substitution of nitrogen for oxygen atoms has been ascribed to the similar ionic radius of a four-coordinated N^{3-} ion (0.132 nm) with an O^{2-} ion (0.124 nm).[9,26] Besides good retention of the crystalline structure, similar morphology (Fig. 1C and S1†) and N_2 adsorption–desorption isotherms (Fig. 1D) are also demonstrated for the samples before and after ammonia treatment. The as-nitrided $Sr_5Ta_4O_{15-x}N_x$ particles are nanoplate aggregates with the width estimated to be *ca.* 50–100 nm, and the surface area is *ca.* 5 $m^2 g^{-1}$. All the results integrally reveal that the thermal ammonia treatment has a minor effect on the structure and morphology of the layered oxide precursor.

Fig. 2A shows the UV-Vis DRS of the $Sr_5Ta_4O_{15}$ and $Sr_5Ta_4O_{15-x}N_x$ samples. Compared with the oxide precursor, the absorption edge of the $Sr_5Ta_4O_{15-x}N_x$ is obviously shifted from 275 to 565 nm, exhibiting extraordinary band-to-band excitation in the visible light region. The band gap of $Sr_5Ta_4O_{15-x}N_x$ is estimated to be 2.20 eV, much smaller than that (4.51 eV) of $Sr_5Ta_4O_{15}$. The extension of visible light absorption is also demonstrated by the color change of the samples from white to bright yellow (see the inset of Fig. 2A). This significantly extended visible light absorption further demonstrates the efficient substitution of nitrogen for oxygen atoms by thermal ammonia treatment. It is worth noting that this large band-to-band red-shift in $Sr_5Ta_4O_{15-x}N_x$, with the steep and almost parallel characteristics for the absorption edge, is different from the commonly observed small absorption shoulders that can only absorb limited visible light.[9,11a]

XPS spectra of N 1s were examined to further confirm the substitution of nitrogen for oxygen atoms. As shown in Fig. 2B, a strong XPS peak centered at 404.0 eV appears in both scans, which is attributed to the abundant Ta $4p_{3/2}$. In contrast to the $Sr_5Ta_4O_{15}$ oxide precursor, two additional peaks centered at 397.5 and 395.5 eV appear for the $Sr_5Ta_4O_{15-x}N_x$ sample. From the previous reports on the nitrogen-doped layered oxides, such as $Sr_2Ta_2O_{7-x}N_x$, $Ba_5Ta_4O_{15-x}N_x$ and $CsCa_2Ta_3O_{10-x}N_x$, it is known that the doped nitrogen with binding energy at *ca.* 395.5 eV can be considered to be atomic β-N, namely the formation of Ta–N bonds in the network of Ta–O–Ta.[14c,15–17] The formation of Ta–N bonds indicates the partial substitution of oxygen with nitrogen atoms in the Ta–O bonds located in the bilayers, leading to the consequent extension of the light absorption region. The origin is understood to be that the species of N/N–H/N–H_2, derived from decomposition of NH_3 molecules, migrate through the interlayer galleries of the $Sr_5Ta_4O_{15}$ and replace the oxygen.[14c] In this work, the molar doping percentage of N/O is evaluated to be *ca.* 4.2% by elemental analysis using a flash elemental analyzer.

The influence of the layered structure on the binding energy of N 1s has been clearly validated in the previous literature.[14a,15] For instance, $Sr_2Ta_2O_{7-x}N_x$ compound with a uniform layered structure shows a single N 1s peak centered at 395.2 eV,[15] while $Cs_{0.68}Ti_{1.83}O_{4-x}N_x$ and $H_{0.68}Ti_{1.83}O_{4-x}N_x$ with the same layered framework exhibit the binding energies of the corresponding nitrogen dopants at 395.0 and 396.2 eV, respectively, due to the different electro-negativities of Cs and H in the interlayer galleries.[14a] As depicted previously, the layered $Sr_5Ta_4O_{15}$ contains two kinds of interlayers, one consists of four strontium ions and the other consists of two strontium ions.[21] It is thus reasonable to ascribe both binding energies (397.5 and 395.5 eV) of the N 1s XPS spectrum of the $Sr_5Ta_4O_{15-x}N_x$ sample to the atomic β-N in consideration of their different layered structures. Compared with the interlayer containing two strontium ions, the interlayer galleries composed of four strontium ions will cause a higher outer electron density around N, which should result in much lower binding energy of N 1s (395.5 eV). In other words, the N 1s peaks with binding energies of 395.5 and 397.5 eV correspond to the atomic β-N in the interlayers with four and two strontium ions, respectively.

The substitution of oxygen with nitrogen atoms was also confirmed by UV Raman spectra of the samples before and after nitridation. In Fig. 2C, there are two characteristic bands at 427 and 792 cm^{-1} in the Raman spectrum of $Sr_5Ta_4O_{15}$, which can be assigned to the vibration of O atoms (E_g(O)

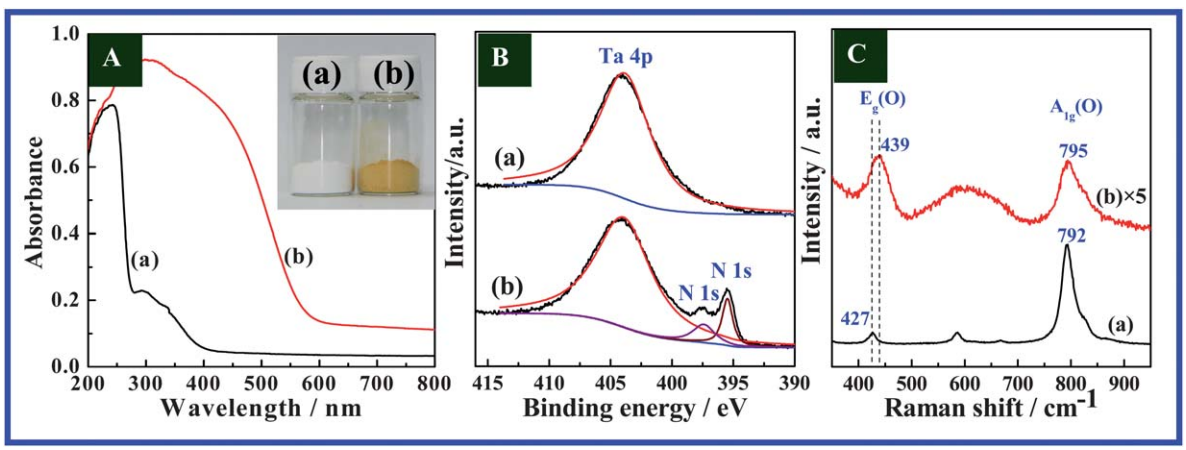

Fig. 2 Spectral characterizations of $Sr_5Ta_4O_{15}$ (a) and $Sr_5Ta_4O_{15-x}N_x$ (b): (A) UV-Vis DRS (inset shows the photos of samples before and after nitridation); (B) XPS spectra; (C) UV Raman spectra.

mode) and the stretching vibrations of TaO_6 octahedron (A_{1g}(O) mode), respectively.[27] After the nitridation treatment, they both shift to higher wavenumbers, with the values of 439 and 795 cm^{-1}, respectively. A similar result was also reported in the nitrogen-doped layered $Cs_{0.68}Ti_{1.83}O_4$.[28] It is known that the vibrational frequency is approximately inversely proportional to the square root of the effective mass of the atoms involved. Hence, the shifts of the E_g(O) and A_{1g}(O) modes to higher wavenumbers reveal the incorporation of N atoms by replacing the O atoms.

Fig. 3 compares the density of states of the samples before and after nitrogen doping. The bottom of the conduction band and the top of the valence band for $Sr_5Ta_4O_{15}$ are dominated by Ta 5d orbitals and O 2p orbitals, respectively. After nitrogen doping, however, the band gap decreases from 1.71 to 1.33 eV due to the mixing of N 2p and O 2p orbitals. The band gap was normally underestimated due to the shortcomings of the exchange–correction functional method in describing excited states, but the predicted narrowing of the band gap is in accordance with the UV-Vis DRS and the color change of the samples. The introduction of N 2p orbital to the top of the valence band for $Sr_5Ta_4O_{15}$ is expected to play a crucial role in extending the absorption into the visible light region.

In order to find the band edge positions of the $Sr_5Ta_4O_{15-x}N_x$, M–S plot of the $Sr_5Ta_4O_{15-x}N_x$ electrode was measured at pH = 8.5 (consistent with the test condition of photocatalytic reaction). According to the intersection point of the potential in Fig. 4, the flat band potential of $Sr_5Ta_4O_{15-x}N_x$ is calculated to be *ca.* −0.48 eV *vs.* NHE in the test condition. It is generally known that the bottom of the conduction bands of n-type semiconductors is more negative by *ca.* −0.1 V than the flat band potential,[29,30] so the band edge positions of the n-type $Sr_5Ta_4O_{15-x}N_x$ are estimated and shown in the inset of Fig. 4, in which both the conduction and valence bands possess sufficient potentials for the water reduction and oxidation, respectively.

3.2 Photocatalytic water splitting performances

The photocatalytic performances of $Sr_5Ta_4O_{15-x}N_x$ for water reduction and oxidation were examined under visible light irradiation in the presence of CH_3OH and $AgNO_3$, respectively. Several typical cocatalysts were employed and deposited to investigate the effect of cocatalysts as well as deposition methods on the performances. The detailed results are given in Table 1. As for water reduction, the parent $Sr_5Ta_4O_{15-x}N_x$ sample without cocatalyst loading does not show any H_2 evolution (entry 1). However, H_2 evolution was obviously observed when the cocatalyst Pt, Rh or Ir was deposited by the impregnation method combined with H_2 reduction

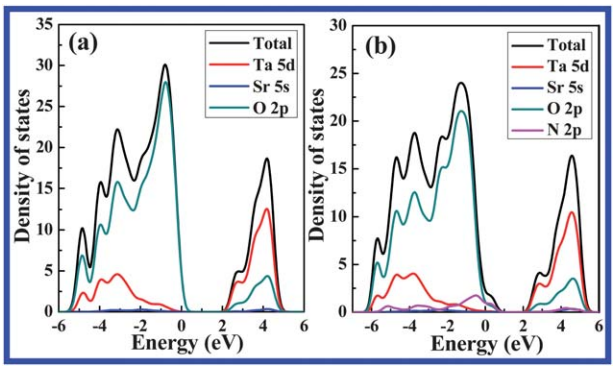

Fig. 3 Density of states of $Sr_5Ta_4O_{15}$ (a) and $Sr_5Ta_4O_{15-x}N_x$ (b).

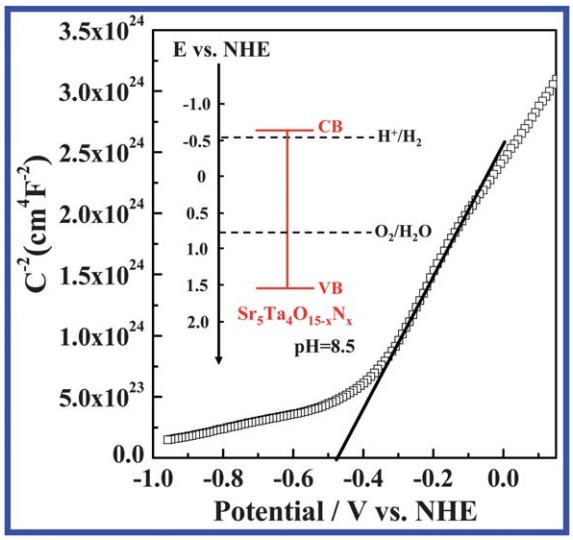

Fig. 4 M–S plot of the $Sr_5Ta_4O_{15-x}N_x$ electrode and the estimated band edge positions of $Sr_5Ta_4O_{15-x}N_x$ at pH = 8.5 (inset). Electrolyte: 0.1 M Na_2SO_4 solution (pH = 8.5, adjusted by NaOH); frequency: 3 kHz.

Table 1 Photocatalytic water splitting performances of the $Sr_5Ta_4O_{15-x}N_x$, $Ba_5Ta_4O_{15-x}N_x$ and $Sr_2Ta_2O_{7-x}N_x$ samples with modified cocatalysts

Entry	Photocatalyst	Cocatalyst[a]	H_2 evolution rate (μmol h^{-1})	O_2 evolution rate (μmol h^{-1})
1	$Sr_5Ta_4O_{15-x}N_x$	None	0	2.4
2		None-H623[b]	0	—
3		Pt(Imp.-H_2)[c]	13.9	—
4		Rh(Imp.-H_2)[c]	9.4	—
5		Ir(Imp.-H_2)[c]	6.9	—
6		None-N973[d]	—	2.3
7		IrO_2	—	7.0
8		CoO_x	—	12.4
9		CoO_x(Imp.)[e]	—	5.5
10	$Ba_5Ta_4O_{15-x}N_x$	None	0	2.4
11		Pt(Imp.-H_2)[c]	12.6	—
12		CoO_x	—	19.9
13	$Sr_2Ta_2O_{7-x}N_x$	None	0	1.8
14		Pt(Imp.-H_2)[c]	5.3	—
15		CoO_x	—	12.8

[a] The loading amount of the cocatalyst is 0.3 wt% for water reduction and 1.0 wt% for water oxidation. [b] $Sr_5Ta_4O_{15-x}N_x$ without cocatalyst deposition was treated under the 5% H_2/Ar flow at 623 K for 2 h. [c] Imp.-H_2: impregnation combined with H_2 reduction. [d] $Sr_5Ta_4O_{15-x}N_x$ was treated under the NH_3 flow at 973 K for 1 h, but without CoO_x deposition. [e] The impregnated powder was calcined at 473 K for 2 h in the air.

(entries 3–5). The H_2 evolution rate is also related to the species of cocatalysts, among which the Pt modified sample (entry 3) shows the highest H_2 evolution rate. The optimized content of the deposited Pt is *ca.* 0.3 wt% (Fig. S2†). The possibility of the promotion effect originating from the H_2 treatment can be ruled out, since the $Sr_5Ta_4O_{15-x}N_x$ without cocatalyst loading subjected to thermal H_2 reduction treatment does not show photocatalytic H_2 evolution (entry 2). Fig. 5 gives a representative time course of H_2 evolution on the Pt(Imp.-H_2)/$Sr_5Ta_4O_{15-x}N_x$, in which the H_2 evolution is steady within the 10 h irradiation, and only a small amount of N_2 was just checked in the initial stage of the reaction. The XRD patterns of the sample before and after the reaction show no noticeable difference except that some diffraction peaks attributable to $La(OH)_3$ appear for the sample after the reaction, indicating good stability of the $Sr_5Ta_4O_{15-x}N_x$ for photocatalytic reaction. Fig. 6 exhibits the dependence of the H_2 evolution rate on the wavelength of the irradiation light, in which the trend of the H_2 evolution rate is consistent with that of UV-Vis DRS, indicating that the photocatalytic H_2 evolution on the $Sr_5Ta_4O_{15-x}N_x$ sample is driven by the visible light.

It should be pointed out that the activity of the photocatalytic water reduction is sensitive to the structures of the deposited cocatalysts, which are generally related to their deposition methods. In this work, we have ever attempted to load the platinum, rhodium or iridium cocatalyst by an *in situ* photodeposition method, but unfortunately no H_2 evolution was detected in all cases, as similarly observed on the nitrogen-doped layered oxide $CsCa_2Ta_3O_{10-x}N_x$.[17] As an example illustration of the structure-sensitive reaction, the Pt(P.D.)/$Sr_5Ta_4O_{15-x}N_x$ and Pt(Pt-Imp.)/$Sr_5Ta_4O_{15-x}N_x$ samples were thus characterized for comparison. Based on the UV-Vis absorption spectra (Fig. S3†) and ICP analysis, a similar content of platinum loaded on both samples can be confirmed. However, the valence states and the morphologies of platinum deposited on the surface of the photocatalyst by these two methods are different according to their binding energies in the XPS spectra (Fig. S4†) and SEM/TEM images (Fig. S5†). The platinum loaded by *in situ* photodeposition is homogeneously dispersed (Fig. S5a and c†) and exists mainly as PtO (Fig. S4†), while the impregnated platinum nanoparticles with the size range of 1–4 nm (Fig. S5b and d†) are randomly observed and known as metallic states (Fig. S4†). It is worth noting that after the sample of Pt(P.D.)/$Sr_5Ta_4O_{15-x}N_x$ was post-reduced under a 5% H_2/Ar flow at 623 K for 2 h (similar to the preparation of Pt(Imp.-H_2)/$Sr_5Ta_4O_{15-x}N_x$) to convert the PtO into metallic platinum, obvious H_2 evolution (3.7 μmol h^{-1}) was also detected. This further confirmed that the formed PtO instead of metallic platinum by the *in situ* photodeposition should be responsible for no H_2 evolution. Metallic platinum is expected to be formed on the Pt(P.D.)/$Sr_5Ta_4O_{15-x}N_x$ sample with post-H_2 reduction, but the morphology of the coated platinum is different from that on the Pt(Imp.-H_2)/$Sr_5Ta_4O_{15-x}N_x$ sample, indicating that the morphology of the metallic platinum is another parameter affecting the photocatalytic H_2 evolution.

Photocatalytic water oxidation involving a four-electron transfer process is a more challenging step than water reduction, and the loading of cocatalyst for the O_2 evolution has been demonstrated to make a great effect on the O_2 evolution.[1b,e,f,22] To evaluate the water oxidation performance of the $Sr_5Ta_4O_{15-x}N_x$, three typical oxidation cocatalysts, namely CoO_x, IrO_2 and CoO_x(Imp.), were thus deposited in this work. As shown in the entries 1 and 6–9 of Table 1, the parent sample

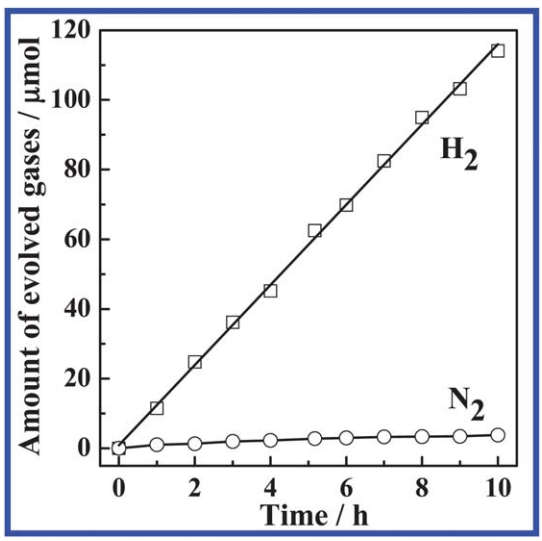

Fig. 5 Typical time course of photocatalytic H_2 evolution on 0.3 wt% Pt/$Sr_5Ta_4O_{15-x}N_x$ under visible light irradiation. *Reaction conditions*: 20 v% methanol solution (150 mL) with 0.15 g catalyst and 0.15 g La_2O_3; 300 W Xe lamp ($\lambda \geq$ 420 nm).

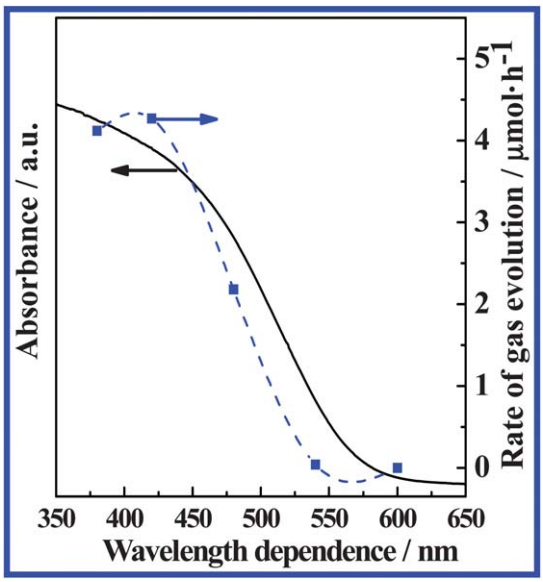

Fig. 6 Dependence of the H_2 evolution rate on the cutoff wavelength of incident light (dotted line) and the UV-Vis DRS of $Sr_5Ta_4O_{15-x}N_x$ (solid line). Experimental conditions: 0.3 wt% Pt/$Sr_5Ta_4O_{15-x}N_x$ (0.15 g); La_2O_3 (0.15 g); 150 mL 20 v% methanol solution system; 1 h irradiation.

without cocatalyst loading can drive water oxidation under visible light irradiation (entry 1), but the loading of cocatalyst makes the water oxidation activity more remarkable (entries 7–9). The promotion effect of the cocatalyst on water oxidation is also dependent on its species and deposition method, and CoO_x is the most efficient one. As shown in Fig. S6,† the deposited CoO_x nanoparticles with the size range estimated to be 5–15 nm are randomly distributed on the surface of $Sr_5Ta_4O_{15-x}N_x$. It should be pointed out that no obviously aggregated CoO_x particles are observed, which is different from the previous observation.[22] It is worth noting that the NH_3 flow thermal treatment of $Sr_5Ta_4O_{15-x}N_x$ without cocatalyst loading does not have any promotion effect on the O_2 evolution (entry 6), indicating its unfavorable contribution to the promotion of O_2 evolution.

Fig. 7 shows the time course of O_2 evolution on the $CoO_x/Sr_5Ta_4O_{15-x}N_x$ sample under visible light irradiation. No reaction took place in the dark, and O_2 was detected only after the light irradiation. The rate of O_2 evolution decreases with increasing reaction time, as has been mainly ascribed to the coverage of the photoreduced Ag particles on the photocatalyst, which hinders the light absorption and decreases the number of active sites available for reaction.[4c] This is typical behavior in photocatalytic water oxidation using $AgNO_3$ as the electron acceptor. A small amount of N_2 originating from the oxidation of the photocatalyst itself was also observed in the initial stage, but it was kept almost constant after 1.5 h irradiation, demonstrating the good photocatalytic stability of the photocatalyst. We also checked the reproducibility of catalytic performances by varying the material batches, and the photocatalytic activities varied within 5%.

Encouraged by the obvious H_2 and O_2 evolution on the nitrogen-doped layered oxide $Sr_5Ta_4O_{15-x}N_x$ under visible light irradiation, we extended the strategy of cocatalyst loading to other nitrogen-doped tantalum-based layered oxides, $Ba_5Ta_4O_{15-x}N_x$ and $Sr_2Ta_2O_{7-x}N_x$. The nitrogen-doped $Ba_5Ta_4O_{15-x}N_x$ and $Sr_2Ta_2O_{7-x}N_x$ materials have been recently reported to have a wide range of visible light absorption and show photocatalytic water reduction for H_2 production, but their water oxidation performances have never been reported.[15,16] The structures of the samples were confirmed by the XRD patterns given in Fig. S7 and S8.† According to the UV-Vis DRS in Fig. 8, the $Ba_5Ta_4O_{15-x}N_x$ and $Sr_2Ta_2O_{7-x}N_x$ show significantly extended visible light absorption compared with their oxide precursors, the absorption edges of which can reach 630 and 560 nm, respectively. As shown in Table 1, the $Ba_5Ta_4O_{15-x}N_x$ and $Sr_2Ta_2O_{7-x}N_x$ materials modified with Pt and CoO_x show obvious H_2 and O_2 evolution activities under visible light irradiation, respectively (entries 10–15). The corresponding time courses of H_2 and O_2 evolution on the $Ba_5Ta_4O_{15-x}N_x$ and $Sr_2Ta_2O_{7-x}N_x$ photocatalysts are given in Fig. S9 and S10.† Considering both H_2 and O_2 evolution on the $Sr_5Ta_4O_{15-x}N_x$ photocatalyst, the nitrogen-doped tantalum-based layered oxides demonstrate good potential in solar water splitting.

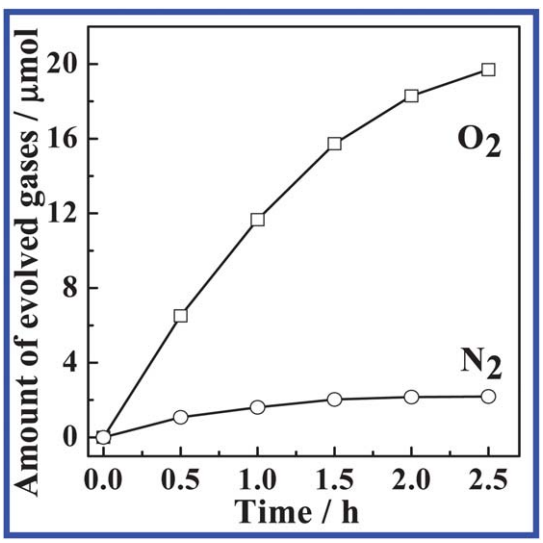

Fig. 7 Typical time course of O_2 evolution on the $CoO_x/Sr_5Ta_4O_{15-x}N_x$ under visible light irradiation. *Reaction conditions*: 0.01 M $AgNO_3$ solution (150 mL); 0.15 g catalyst; 0.15 g La_2O_3; 300 W Xe lamp ($\lambda \geq 420$ nm).

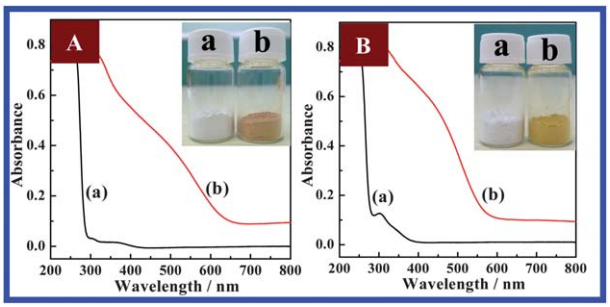

Fig. 8 UV-Vis DRS and photos (inset) of the samples before and after nitridation: (A) $Ba_5Ta_4O_{15}$ (a) and $Ba_5Ta_4O_{15-x}N_x$ (b); (B) $Sr_2Ta_2O_7$ (a) and $Sr_2Ta_2O_{7-x}N_x$ (b).

4 Conclusions

Here we developed a novel nitrogen-doped layered oxide $Sr_5Ta_4O_{15-x}N_x$ *via* a thermal ammonalysis process, which can not only harvest a wide range of visible light, but also obviously drive both water reduction and oxidation half reactions under visible light irradiation. Compared with the oxide precursor of $Sr_5Ta_4O_{15}$, the broad extension of visible light absorption has been ascribed to the efficient substitution of nitrogen for oxygen atoms, confirmed by various characterizations and theoretical calculation. The thermodynamic feasibility of water reduction and oxidation on the $Sr_5Ta_4O_{15-x}N_x$ sample was also confirmed by combining UV-Vis DRS with M-S measurement. The photocatalytic water splitting performances are sensitive to the structure of the deposited cocatalysts which is influenced by the deposition methods. With the modification of the cocatalyst Pt or CoO_x, the nitrogen-doped tantalum-based layered oxides $Ba_5Ta_4O_{15-x}N_x$ and $Sr_2Ta_2O_{7-x}N_x$ with narrow band gaps of *ca.* 1.97 and 2.22 eV can also evolve H_2 or O_2. To the best of our knowledge, for the first time, the nitrogen-doped

tantalum-based layered oxides are proved to be active in the visible light range for two half reactions of water splitting. This strategy of the nitrogen doping is also expected to develop more photocatalysts with a large range of visible light utilization for solar water splitting.

Acknowledgements

This work was financially supported by National Natural Science Foundation of China (No. 21090340); Solar Energy Action Plan of Chinese Academy of Sciences (ACS).

Notes and references

1 (*a*) J. S. Lee, *Catal. Surv. Asia*, 2005, **9**, 217; (*b*) K. Maeda and K. Domen, *J. Phys. Chem. C*, 2007, **111**, 7851; (*c*) A. Kudo and Y. Miseki, *Chem. Soc. Rev.*, 2009, **38**, 253; (*d*) P. V. Kamat, *J. Phys. Chem. C*, 2007, **111**, 2834; (*e*) Y. Inoue, *Energy Environ. Sci.*, 2009, **2**, 364; (*f*) K. Maeda and K. Domen, *J. Phys. Chem. Lett.*, 2010, **1**, 2655.

2 (*a*) F. E. Osterloh, *Chem. Mater.*, 2008, **20**, 35; (*b*) X. B. Chen, S. H. Shen, L. J. Guo and S. S. Mao, *Chem. Rev.*, 2010, **110**, 6503; (*c*) H. Tong, S. X. Ouyang, Y. P. Bi, N. Umezawa, M. Oshikiri and J. H. Ye, *Adv. Mater.*, 2012, **24**, 229.

3 (*a*) D. Dvoranova, V. Brezova, M. Mazur and M. A. Malati, *Appl. Catal., B*, 2002, **37**, 91; (*b*) K. Iwashina and A. Kudo, *J. Am. Chem. Soc.*, 2011, **133**, 13272; (*c*) S. X. Ouyang, H. Tong, N. Umezawa, J. Cao, P. Li, Y. P. Bi, Y. J. Zhang and J. H. Ye, *J. Am. Chem. Soc.*, 2012, **134**, 1974.

4 (*a*) G. Hitoki, T. Takata, J. N. Kondo, M. Hara, H. Kobayashi and K. Domen, *Chem. Commun.*, 2002, **16**, 1698; (*b*) G. Hitoki, A. Ishikawa, T. Takata, J. N. Kondo, M. Hara and K. Domen, *Chem. Lett.*, 2002, **7**, 736; (*c*) A. Kasahara, K. Nukumizu, G. Hitoki, T. Takata, J. N. Kondo, M. Hara, H. Kobayashi and K. Domen, *J. Phys. Chem. A*, 2002, **106**, 6750; (*d*) K. Maeda, K. Teramura, D. L. Lu, T. Takata, N. Saito, Y. Inoue and K. Domen, *Nature*, 2006, **440**, 295; (*e*) M. Higashi, R. Abe, T. Takata and K. Domen, *Chem. Mater.*, 2009, **21**, 1543; (*f*) X. Wang, K. Maeda, A. Thomas, K. Takanabe, G. Xin, J. M. Carlsson, K. Domen and M. Antonietti, *Nat. Mater.*, 2009, **8**, 76; (*g*) B. Siritanaratkul, K. Maeda, T. Hisatomi and K. Domen, *ChemSusChem*, 2011, **4**, 74.

5 (*a*) K. Kalyanasundaram, E. Borgarello, D. Duonghong and M. Graetzel, *Angew. Chem., Int. Ed. Engl.*, 1981, **20**, 987; (*b*) A. Ishikawa, T. Takata, J. N. Kondo, M. Hara, H. Kobayashi and K. Domen, *J. Am. Chem. Soc.*, 2002, **124**, 13547; (*c*) A. Ishikawa, T. Takata, T. Matsumura, J. N. Kondo, M. Hara, H. Kobayashi and K. Domen, *J. Phys. Chem. B*, 2004, **108**, 2637.

6 (*a*) R. G. Breckenridge and W. R. Hosler, *Phys. Rev.*, 1953, **91**, 793; (*b*) D. C. Cronemeyer, *Phys. Rev.*, 1959, **113**, 1222; (*c*) X. B. Chen, L. Liu, Y. Y. Peter and S. S. Mao, *Science*, 2011, **331**, 746; (*d*) X. Xu, C. Randorn, P. Efstathiou and J. T. S. Irvine, *Nat. Mater.*, 2012, **11**, 595.

7 (*a*) M. Hara, J. Nunoshige, T. Takata, J. N. Kondo and K. Domen, *Chem. Commun.*, 2003, 3000; (*b*) K. Maeda, M. Higashi, D. L. Lu, R. Abe and K. Domen, *J. Am. Chem. Soc.*, 2010, **132**, 5858; (*c*) M. Higashi, K. Domen and R. Abe, *J. Am. Chem. Soc.*, 2012, **134**, 6968.

8 (*a*) K. Maeda, T. Takata, M. Hara, N. Saito, Y. Inoue, H. Kobayashi and K. Domen, *J. Am. Chem. Soc.*, 2005, **127**, 8286; (*b*) K. Maeda, K. Teramura, D. L. Lu, N. Saito, Y. Inoue and K. Domen, *Angew. Chem., Int. Ed.*, 2006, **118**, 7970; (*c*) T. Ohno, L. Bai, T. Hisatomi, K. Maeda and K. Domen, *J. Am. Chem. Soc.*, 2012, **134**, 8254.

9 R. Asahi, T. Morikawa, T. Ohwaki, K. Aoki and Y. Taga, *Science*, 2001, **293**, 269.

10 (*a*) T. Lindgren, J. M. Mwabora, E. Avendano, J. Jonsson, A. Hoel, C. G. Granqvist and S. E. Lindquist, *J. Phys. Chem. B*, 2003, **107**, 5709; (*b*) S. Yin, H. Yamaki, M. Komatsu, Q. W. Zhang, J. S. Wang, Q. Tang, F. Saito and T. Sato, *J. Mater. Chem.*, 2003, **13**, 2996; (*c*) Y. N. Huo, Z. F. Bian, X. Y. Zhang, Y. Jin, J. Zhu and H. X. Li, *J. Phys. Chem. C*, 2008, **112**, 6546.

11 (*a*) D. Li and H. Haneda, *J. Photochem. Photobiol., A*, 2003, **155**, 171; (*b*) H. Irie, Y. Watanabe and K. Hashimoto, *J. Phys. Chem. B*, 2003, **107**, 5483.

12 C. Burda, Y. B. Lou, X. B. Chen, A. C. S. Samia, J. Stout and J. L. Gole, *Nano Lett.*, 2003, **3**, 1049.

13 (*a*) M. Miyauchi, M. Takashio and H. Tobimatsu, *Langmuir*, 2004, **20**, 232; (*b*) G. Liu, L. C. Yin, J. Q. Wang, P. Niu, C. Zhen, Y. P. Xie and H. M. Cheng, *Energy Environ. Sci.*, 2012, **5**, 9603.

14 (*a*) G. Liu, L. Z. Wang, C. H. Sun, X. X. Yan, X. W. Wang, Z. G. Chen, S. C. Smith, H. M. Cheng and G. Q. Lu, *Chem. Mater.*, 2009, **21**, 1266; (*b*) G. Liu, L. Z. Wang, H. G. Yang, H. M. Cheng and G. Q. Lu, *J. Mater. Chem.*, 2010, **20**, 831; (*c*) A. Mukherji, R. Marschall, A. Tanksale, C. H. Sun, S. C. Smith, G. Q. Lu and L. Z. Wang, *Adv. Funct. Mater.*, 2011, **21**, 126; (*d*) S. Cho, J. W. Jang, K. Kong, E. S. Kim, K. H. Lee and J. S. Lee, *Adv. Funct. Mater.*, 2013, DOI: 10.1002/adfm.201201883.

15 A. Mukherji, B. Seger, G. Q. Lu and L. Z. Wang, *ACS Nano*, 2011, **5**, 3483.

16 A. Mukherji, C. H. Sun, S. C. Smith, G. Q. Lu and L. Z. Wang, *J. Phys. Chem. C*, 2011, **115**, 15674.

17 X. Zong, C. H. Sun, Z. G. Chen, A. Mukherji, H. Wu, J. Zou, S. C. Smith, G. Q. Lu and L. Z. Wang, *Chem. Commun.*, 2011, **47**, 6293.

18 S. Ida, Y. Okamoto, M. Matsuka, H. Hagiwara and T. Ishihara, *J. Am. Chem. Soc.*, 2012, **124**, 15773.

19 H. Kato, K. Asakura and A. Kudo, *J. Am. Chem. Soc.*, 2003, **125**, 3082.

20 K. Maeda and K. Domen, *Angew. Chem., Int. Ed.*, 2012, **51**, 9865.

21 K. Yoshioka, V. Petrykin, M. Kakihana, H. Kato and A. Kudo, *J. Catal.*, 2005, **232**, 102.

22 F. X. Zhang, A. Yamakata, K. Maeda, Y. Moriya, T. Takata, J. Kubota, K. Teshima, S. Oishi and K. Domen, *J. Am. Chem. Soc.*, 2012, **134**, 8348.
23 F. X. Zhang, K. Maeda, T. Takata, T. Hisatomi and K. Domen, *Catal. Today*, 2012, **185**, 253.
24 G. Kresse and J. Furthmüller, *Phys. Rev. B: Condens. Matter Mater. Phys.*, 1996, **54**, 169.
25 G. Kresse and D. Joubert, *Phys. Rev. B: Condens. Matter Mater. Phys.*, 1999, **59**, 1758.
26 R. D. Shannon, *Acta Crystallogr., Sect. A: Cryst. Phys., Diffr., Theor. Gen. Crystallogr.*, 1976, **32**, 751.
27 C. T. Chia, Y. C. Chen, H. F. Cheng and I. N. Lin, *J. Appl. Phys.*, 2003, **94**, 3360.
28 G. Liu, P. Niu, L. Wang, G. Q. Lu and H. M. Cheng, *Catal. Sci. Technol.*, 2011, **1**, 222.
29 Y. Matsumoto, K. Omae, I. Watanabe and E. Sato, *J. Electrochem. Soc.*, 1986, **133**, 711.
30 Y. Matsumoto, *J. Solid State Chem.*, 1996, **126**, 227.